Research Square

Preprints are preliminary reports that have not undergone peer review.
They should not be considered conclusive, used to inform clinical practice,
or referenced by the media as validated information.

Docking and Molecular Dynamics of the Natural Diterpenoid Dihydrotanshinone I in Human 15-PGDH Across Three Inhibitor-Bound Receptor Structures

Sabbir Ahmad Antor
Shahjalal University of Science and Technology https://orcid.org/0009-0008-4020-2316
Md Abu Sadat Soash
Shahjalal University of Science and Technology https://orcid.org/0009-0001-1116-2449
Muktadir Al Mahmud
Shahjalal University of Science and Technology
Raphael Kabir Niloy
Shahjalal University of Science and Technology https://orcid.org/0009-0006-4907-4221
Md. Mainul Hossain Bakul
Shahjalal University of Science and Technology https://orcid.org/0009-0003-2929-6271
Gokul Chandra Biswas
gcbiswas-geb@sust.edu
Shahjalal University of Science and Technology https://orcid.org/0000-0001-9097-6426

Research Article

Keywords:

Posted Date: August 18th, 2026

DOI: https://doi.org/10.21203/rs.3.rs-10719902/v1

License: This work is licensed under a Creative Commons Attribution 4.0 International License.
Read Full License

Additional Declarations: The authors declare no competing interests.

Abstract

15-hydroxyprostaglandin dehydrogenase (15-PGDH) is the enzyme that inactivates prostaglandin E2, and its inhibition raises prostaglandin E2 and rejuvenates aged skeletal muscle, which makes it an attractive target for age-related muscle decline. Although natural products are documented functional inhibitors of 15-PGDH, almost none has been characterized by structure-based docking, and the tanshinones of *Salvia miltiorrhiza* have not been examined against this enzyme. Here, dihydrotanshinone I, with panaxynol as a comparator, was docked into three experimentally determined 15-PGDH structures, the X-ray cocrystals 9PFL and 9PFM and the cryo-electron microscopy structure 8CVN, using a protocol validated for each receptor by redocking its own crystallographic inhibitor (heavy-atom RMSD 0.38 to 1.46 Angstrom). Dihydrotanshinone I docked favourably into the inhibitor pocket of all three structures, with best predicted docking affinities of − 8.94 to − 10.5 kcal/mol. In the X-ray structures, it formed a hydrogen bond with catalytic Ser138 and contacted Tyr151 and the lid-hinge residue Phe185, whereas in the cryo-electron microscopy structure it was anchored by Phe185 and Tyr217.Across fifteen independent random seeds the top pose was highly reproducible in every structure, with maximum pairwise RMSDs below 0.2 Angstrom, confirming that it is the dominant docking solution and not a seed-dependent artefact. The precise orientation was only partly conserved across the ensemble, so a single rigid binding mode is not established by docking alone. Triplicate 100 ns molecular dynamics simulations of all three complexes, nine trajectories in total, showed that the compound remained in continuous contact with the protein throughout every run and retained its contacts with the inhibitor-site residues, that Phe185 is contacted in essentially every frame while Lys155 is contacted in none, and that the three docked poses remained largely distinct under receptor flexibility, with one 8CVN replica of nine relocating toward the 9PFL pose. These three results were unchanged when recomputed across equilibration discard windows of 0 to 50 ns. Together the docking and the simulations identify dihydrotanshinone I as a reproducible, mechanistically plausible natural-compound candidate for the 15-PGDH inhibitor pocket. Predicted binding is reported as an estimate of binding potential and not as proven enzyme inhibition.

1. Introduction

The loss of skeletal muscle mass and strength with age, sarcopenia, contributes to frailty, falls, and loss of independence, and has no approved pharmacological treatment. One molecular node whose modulation can reverse age-related muscle decline is the eicosanoid mediator prostaglandin E2, which supports muscle stem cell function and regeneration. The intracellular level of prostaglandin E2 is set not only by its cyclooxygenase-dependent synthesis but also by its catabolism, and the committed catabolic step is carried out by 15-hydroxyprostaglandin dehydrogenase (15-PGDH), an NAD(+)-dependent oxidoreductase that oxidises prostaglandin E2 to its inactive 15-keto form. Because raising prostaglandin E2 is beneficial in ageing muscle, inhibition of the degrading enzyme is a rational strategy, and genetic or small-molecule inhibition of 15-PGDH has been shown to restore mass, strength, and mitochondrial function in aged muscle (Palla et al., 2021).

15-PGDH belongs to the short-chain dehydrogenase/reductase superfamily and acts as a homodimer, with each protomer binding the NAD(+) cofactor in a Rossmann fold adjacent to the substrate pocket. Three well-conserved residues, Ser138, Tyr151, and Lys155, have been shown to form the catalytic triad (Zhou et al., 2001), and the crystal structure of the enzyme bound to NAD(+) was used to rationalise the mechanisms of its early inhibitors (Niesen et al., 2010). More recently, cryo-electron microscopy resolved 15-PGDH bound to inhibitors and revealed a dynamic lid domain that closes over the pocket, with Phe185 and Tyr217 acting as hinges that potent inhibitors exploit (Huang et al., 2023), and high-resolution X-ray cocrystals of the enzyme with designed inhibitors were subsequently deposited (Dodda et al., 2025). This induced-fit behaviour identifies the residues a credible docked pose should contact and defines a clear limitation of rigid-receptor docking.

15-PGDH is a well-validated target with a mature medicinal-chemistry programme. The prototype inhibitor SW033291 inhibits the enzyme with sub-nanomolar potency, roughly doubles prostaglandin E2 in vivo, and promotes tissue regeneration in several organs (Zhang et al., 2015). By contrast, the natural-product side is thin. The best-characterised botanical inhibitor is panaxynol, which inhibits 15-PGDH noncompetitively (Fujimoto et al., 1998), but the structural and computational characterisation of defined natural inhibitors is almost absent, the only prior natural-compound computational effort being a high-throughput screen of anonymous library entries (Ahmad et al., 2024). This asymmetry, functional evidence for natural inhibition without structural characterisation, is the opening this study addresses.

Dihydrotanshinone I is the principal lipophilic phenanthraquinone of *Salvia miltiorrhiza* (Danshen), a rigid abietane diterpenoid with documented antioxidant, anti-inflammatory, and antitumour activity and defined molecular targets (Yue et al., 2024). Three properties make it a strong docking candidate: it is structurally rigid with a low rotatable-bond count, which keeps the search tractable; it has demonstrated, specific target engagement, not only diffuse antioxidant activity; and its anti-inflammatory pharmacology places it in the same signalling neighbourhood as the prostaglandin E2 axis that 15-PGDH governs. Network pharmacology and macrophage assays identify PTGS2, the inducible cyclooxygenase upstream of prostaglandin E2, among the principal inflammation targets of the closely related tanshinone I (Cui et al., 2020). No tanshinone has been reported to have been docked into 15-PGDH.

This study therefore docks dihydrotanshinone I, with panaxynol as a mechanistically distinct comparator, into three inhibitor-bound conformations of human 15-PGDH, validates the protocol by redocking each structure's own inhibitor, and tests reproducibility across independent random seeds. The guiding hypothesis is that dihydrotanshinone I can occupy the structurally characterised inhibitor-binding region and engage residues involved in substrate recognition (Ser138, Tyr151) and in stabilising the induced-fit lid (Phe185, Tyr217). The work is framed as a structure-based assessment of binding potential and mechanistic plausibility; docking predicts binding and cannot by itself prove enzyme inhibition.

2. Materials and methods

2.1. Protein structures and receptor preparation

Three experimentally determined structures of human 15-PGDH were retrieved from the RCSB Protein Data Bank (Burley et al., 2023) and used together as a small ensemble of inhibitor-bound receptor conformations, so that binding could be judged across more than one static snapshot of the enzyme. The set comprised the X-ray cocrystal structures 9PFL and 9PFM (Dodda et al., 2025) and the cryo-electron microscopy structure 8CVN (Huang et al., 2023), each solved with a bound small-molecule inhibitor and its nicotinamide cofactor. The ensemble was intentionally restricted to experimentally determined inhibitor-bound conformations so that every receptor could undergo structure-specific redocking validation against its own crystallographic ligand. This design prioritises validated inhibitor-pocket geometry over maximal conformational diversity, and it therefore does not sample an unoccupied, apo-like state such as the NAD(+)-bound structure 2GDZ (Niesen et al., 2010), which is used here only as a mechanistic reference. Coordinate files were downloaded in mmCIF format, since the legacy PDB format is no longer generated for some of these depositions, and parsed with gemmi (Wojdyr, 2022).

15-PGDH is a homodimer in which each protomer carries its own cofactor and, in these structures, its own bound inhibitor. 9PFL and 8CVN are deposited as the two-chain assembly and 9PFM as a single chain. In the two two-chain depositions the opposing protomer lay more than 6 Angstrom from the inhibitor bound to chain A and did not line the pocket, so a single protomer together with its own cofactor was used as the docking receptor in every case, matching the content of the 9PFM deposition. Crystallographic waters, ions, glycerol, and ethylene glycol were removed. The cofactor was kept, because the substrate pocket sits immediately against it, and its bond orders and protonation state were rebuilt from the RCSB chemical component SMILES using RDKit (Landrum, n.d.), giving NAD for 9PFL and 9PFM and NADH for 8CVN. Residues with alternate conformers were resolved to a single altloc. Polar hydrogens were added and Gasteiger partial charges (Gasteiger & Marsili, 1980) were assigned during receptor preparation with Meeko (Forli Lab, n.d.), and each protein plus its cofactor was written out as a single rigid receptor in PDBQT format. The structures are summarised in Table 1.

Table 1
Human 15-PGDH structures used as the docking ensemble. Resolutions are in Angstrom and are taken from the deposited coordinate files; the cryo-EM value of 2.40 is the reported map resolution at the FSC 0.143 criterion.

PDB ID	Method	Resolution	Cofactor	Co-crystallized inhibitor	Role
9PFL	X-ray	1.65	NAD	A1CH2 (C21H21F2N5O3)	Primary inhibitor-bound receptor
9PFM	X-ray	1.88	NAD	SWL (C19H23N5OS3)	Independent X-ray receptor
8CVN	Cryo-EM	2.40	NADH	SWL / SW209415	Independent, lid-closed conformation

2.2. Ligand and reference-inhibitor preparation

The candidate ligand dihydrotanshinone I and the comparator panaxynol (falcarinol) were retrieved from PubChem (Kim et al., 2023) and confirmed against the expected molecular formula and mass (Table 2). Each structure's own co-crystallized inhibitor was extracted from its coordinate file for redocking. Three-dimensional coordinates were taken from PubChem, hydrogens were added, and the geometry was relaxed with the Merck molecular force field (Halgren, 1996) in RDKit, and every ligand was converted to PDBQT with Meeko.

Table 2
Identity confirmation of the docked ligands.

Compound	Role	PubChem CID	Formula	MW (g/mol)
Dihydrotanshinone I	Candidate	11425923	C18H14O3	278.3
Panaxynol (falcarinol)	Comparator	5281149	C17H24O	244.4

2.3. Binding site definition and docking grid

For each receptor, the search space was centred on the centroid of that structure's own co-crystallized inhibitor and defined as a cube 24 Angstrom on a side. Centring the box on the experimentally observed inhibitor position anchors the search on a region already known to be the binding site, and holding the box size fixed across the three receptors keeps the scores comparable between structures.

2.4. Redocking validation

Before any candidate compound was docked, the protocol was validated separately for each receptor by extracting its own crystallographic inhibitor and redocking it. Agreement between the top-scoring redocked pose and the crystallographic pose was measured as the heavy-atom RMSD, with atom correspondence guaranteed because the redocked ligand and the reference pose share the same prepared file and atom order. A redock within approximately 2 Angstrom was treated as evidence that the preparation and grid reproduce the true binding mode. The same 2 Angstrom criterion was applied to all three receptors, including the cryo-electron microscopy structure. The redocking accuracy obtained tracks the resolution of the source structure across the ensemble (Tables 1 and 3), which is expected if the achievable agreement is limited in part by the precision with which the crystallographic ligand itself is placed.

2.5. Molecular docking

Docking was carried out with AutoDock Vina 1.2.7 (Eberhardt et al., 2021; Trott & Olson, 2010) using an exhaustiveness of 32 and keeping the nine best-scoring poses from each run. To assess how far the reported affinities depend on the scoring function, the top-ranked pose of each ligand in each receptor was afterwards rescored in score-only mode, without re-docking and with the original search box, under both the default Vina function and Vinardo (Quiroga & Villarreal, 2016); the Vina score was additionally decomposed into its intermolecular and torsional contributions as reported by the program. Dihydrotanshinone I and panaxynol were each docked into all three receptors under identical settings,

and binding was judged from the best predicted affinity together with the contacts of the top-ranked pose. Predicted affinities are used only as a relative estimate of binding potential and are not read as measured inhibition constants.

2.6. Protein-ligand interaction analysis

Interactions of each top-ranked pose were characterised two independent ways so that one method could check the other. The Protein-Ligand Interaction Profiler, PLIP (Schake et al., 2025), was used to detect hydrogen bonds, hydrophobic contacts, pi-stacking, and halogen bonds, and this was cross-checked with an atom-pairwise scan reporting every receptor residue with any atom within 4 Angstrom of the ligand. Five residues defining the catalytic and inhibitor-binding environment were flagged: the catalytic residues Ser138, Tyr151, and Lys155, and the lid-hinge residues Phe185 and Tyr217. Because crystallographic numbering can differ between depositions, correspondence of these residues across all three structures was confirmed by pairwise global sequence alignment with Biopython (Cock et al., 2009) before contacts were compared. Format conversion used Open Babel (O'Boyle et al., 2011) and molecular visualisation used PyMOL (Schrodinger, LLC, n.d.).

2.7. Cross-conformation and reproducibility analysis

To test whether dihydrotanshinone I binds in a consistent orientation across the three conformations, the protomers were superposed onto a common frame using their shared backbone C-alpha atoms and least-squares Kabsch fitting (Kabsch, 1976), with 9PFL as reference, and the same rigid-body transform was applied to each structure's docked top pose. Consistency was expressed as the pairwise heavy-atom RMSD between the transformed poses and, separately, as the distance between their centroids, so that a difference in overall location could be distinguished from a difference in orientation. To test whether the top pose was dependent on the random seed of the search, dihydrotanshinone I was redocked fifteen times into each structure with different seeds under otherwise identical settings; the fifteen top poses were clustered by pairwise heavy-atom RMSD, and the spread of affinities and the persistence of the flagged contacts were recorded.

2.8. Molecular dynamics simulations

To relax the rigid-receptor approximation and test the dynamic persistence of the docked poses, each of the three docked complexes was simulated in explicit solvent in triplicate, giving nine 100 ns replicate trajectories. Simulations were run with GROMACS 2026.3 (Abraham et al., 2015). The protein was described with the AMBER ff14SB force field (Maier et al., 2015), and dihydrotanshinone I with GAFF2 using AM1-BCC partial charges (Wang et al., 2004; Jakalian et al., 2002), assigned with antechamber and parmchk2 from AmberTools (Case et al., 2023). The nicotinamide cofactor was described with the published AMBER parameter set distributed with AmberTools, in which the partial charges were derived by restrained electrostatic potential fitting and the bonded parameters were adapted from the CHARMM parameters of Pavelites et al. (1997) by Walker et al. (2002). Because that set uses generic sequential atom names rather than the chemical-component names of the deposited structures, the two naming schemes were reconciled by graph isomorphism on element-typed connectivity graphs derived

independently from the library connectivity table and from the extracted coordinates, giving a unique assignment for every heavy atom other than the chemically equivalent non-bridging phosphate oxygens, and the renamed libraries were verified to cover all 44 cofactor heavy atoms in each system. The cofactor was modelled in its physiological charge state, NAD carrying a net charge of -1 in 9PFL and 9PFM and NADH a net charge of -2 in 8CVN, not the formally neutral state of the deposited chemical component. This parameter set was developed for the ff94 and ff99 force fields and is used here with ff14SB. As for docking, a single protomer with its own cofactor was simulated. In 9PFL and 8CVN the second chain lies more than 6 Angstrom from the bound inhibitor and does not line the pocket, so it was omitted; 9PFM is deposited as a single chain. This leaves the interface of the physiological homodimer unsatisfied in all three systems. Systems were assembled with tleap, which added hydrogens at the standard ionisation states for neutral pH: all five histidines were assigned the neutral epsilon tautomer, aspartate and glutamate were left deprotonated, lysine and arginine protonated, and the four cysteines left free, no disulfide being present. No residue-specific pKa calculation was performed. The 8CVN sample was prepared at pH 7.4, consistent with these assignments. The assembled systems were converted to GROMACS format with acpype (Sousa da Silva & Vranken, 2012), solvated in TIP3P water (Jorgensen et al., 1983) with at least 10 Angstrom padding, neutralised and brought to 0.15 M NaCl using the monovalent ion parameters of Joung and Cheatham (2008), with ions placed at random positions, giving final system sizes of 32,448, 36,016 and 34,694 atoms for 9PFL, 9PFM and 8CVN respectively.

Each system was energy-minimised by steepest descent, equilibrated for 100 ps in the NVT ensemble with position restraints of 1000 kJ per mol per nm squared on protein, cofactor and ligand heavy atoms, then equilibrated through four consecutive 250 ps NPT stages in which those restraints were released stepwise at 1000, 500 and 200 kJ per mol per nm squared and finally removed altogether. Production was 100 ns per replica with no restraints. All stages used a 2 fs timestep with bonds to hydrogen constrained by LINCS (Hess et al., 1997), the Verlet cutoff scheme with a 1.0 nm cutoff for both van der Waals and short-range electrostatics, particle-mesh Ewald for long-range electrostatics (Darden et al., 1993) with 0.12 nm Fourier spacing and fourth-order interpolation, and a long-range dispersion correction applied to both energy and pressure. Temperature was held at 300 K with the velocity-rescaling thermostat (Bussi et al., 2007) using a 0.1 ps coupling constant and separate coupling groups for the solute and for solvent plus ions. Pressure was held at 1 bar with isotropic coupling, a 2.0 ps coupling constant and a compressibility of 4.5 by 10 to the power − 5 per bar, using the stochastic cell-rescaling barostat (Bernetti & Bussi, 2020) during the restrained NPT stages and the Parrinello-Rahman barostat (Parrinello & Rahman, 1981) once restraints were released and throughout production. Wherever position restraints were combined with pressure coupling, reference-coordinate scaling was applied so that restraint reference positions scaled with the box. Coordinates were saved every 10 ps, giving 10,001 frames per trajectory.

The three replicas of each system were initiated from the same solvated build and differ only in their initial velocities, which were generated from a new random seed at the NVT stage of each replica. That

the velocity sets are genuinely distinct was confirmed directly, by verifying that the initial velocities differ atom by atom between replicas, not by comparing seed values alone.

2.9. Trajectory analysis

Trajectories were corrected for periodic boundary effects before any measurement, first making molecules whole and centring on the protein, then removing jumps. This step is not cosmetic: the uncorrected trajectories contain apparent ligand displacements of up to 9.8 nm that are entirely artefactual, and every trajectory was checked to confirm the artefact had been removed before any distance was measured. Ligand root-mean-square deviation was computed after least-squares fitting on protein backbone atoms, never on the ligand itself. Contacts were measured with the same convention used for the docked poses, the minimum heavy-atom distance between the complete residue and the complete ligand with a 4 Angstrom cutoff, so that occupancies are directly comparable with Table 5; the docked-pose distances in Table 5 were themselves confirmed by an independently written script reading the receptor and pose coordinate files directly; occupancy is the percentage of analysed frames satisfying that criterion. This threshold is the inter-heavy-atom distance PLIP uses to define a hydrophobic contact (Salentin et al., 2015), and it sits at the conservative end of the 4 to 5 Angstrom range conventionally applied to residue-level contact analysis of simulation trajectories. Retention was scored by a separate and deliberately permissive criterion: a frame counted as retained when the minimum heavy-atom distance between the ligand and any protein atom was 4.5 Angstrom or less. That criterion tests only that the ligand stayed in contact with the protein and does not by itself establish occupancy of the inhibitor site; assignment of the ligand to the inhibitor-site region is supported instead by the residue-level contact occupancy and the ligand RMSD reported alongside it. Hydrogen bonding to Ser138 was assessed separately using geometric criteria, a donor-acceptor distance of 0.35 nm or less together with a deviation from linearity of 30 degrees or less. Equilibration discard windows were determined for each trajectory from the point at which its own backbone RMSD plateaued rather than by a fixed rule. Because that determination is made by inspection, the sensitivity of every occupancy to the choice was tested by recomputing it at discard windows of 0, 10, 20, 30 and 50 ns; the occupancies reported in Table 10 are those computed over the full production run, and the outcome of the sensitivity test is given in Section 3.9. To test whether the 8CVN ligand relaxed toward the binding mode seen in the X-ray structures, each frame was superposed on a common reference using the 255 shared C-alpha atoms and least-squares fitting (Kabsch, 1976), the same transform was applied to the ligand, and its heavy-atom RMSD and centroid distance from the 9PFL docked pose were followed over time. Ligand internal geometry was assessed as the heavy-atom RMSD obtained when fitting on the ligand itself, which removes overall translation and rotation and therefore reports only internal deformation. Quinone-ring planarity was measured as the improper dihedral across the ring, and out-of-plane deviation at a given centre is reported as the absolute deviation of that improper from planarity, averaged over frames; where such a value is compared against a reference, the reference is the same quantity measured on a parameterised aromatic centre in the same trajectory. Protein radius of gyration was computed over all protein atoms.

3. Results

3.1. Receptor ensemble and the flagged binding-site residues

The three structures represent inhibitor-bound states of the same fold. Superposing 9PFM and 8CVN onto 9PFL gave small backbone deviations of 0.395 Angstrom and 0.725 Angstrom respectively over 255 shared C-alpha atoms, so the ensemble samples closely related global conformations that differ locally in the pocket and lid region and not substantially different folds, even though one structure was solved by cryo-electron microscopy and two by X-ray crystallography. Sequence alignment confirmed that the five flagged residues occupy identical positions in the canonical numbering of all three depositions, so contacts identified in one structure can be compared directly with another. Figure 1 shows the empty pocket of 9PFL with the bound cofactor and the flagged residues.

3.2. Redocking validation

The protocol reproduced the crystallographic binding mode in all three structures (Table 3). The redocked inhibitor came to rest 0.379 Angstrom from its crystal pose in 9PFL, 0.564 Angstrom in 9PFM, and 1.462 Angstrom in 8CVN, all within the tolerances above. In 9PFL the redocked pose recovered the expected hydrogen bonds to Ser138 and Tyr151 and pi-stacking with Phe185 and Tyr217 (Table 6), which shows that the protocol recovers the correct pattern of interactions and not merely a similar overall position. Because the redock reproduces the right chemistry at the right residues, the atom correspondence underlying the RMSD is confirmed by the result itself.

Table 3
Redocking validation across the three structures.

Structure	Method	Redock affinity (kcal/mol)	RMSD to crystal (Angstrom)	Pass
9PFL	X-ray	-13.61	0.379	Yes
9PFM	X-ray	-8.85	0.564	Yes
8CVN	Cryo-EM	-8.82	1.462	Yes

3.3. Docking of dihydrotanshinone I

Dihydrotanshinone I docked favourably into the inhibitor pocket in all three conformations, with best predicted affinities of -8.94, -9.56, and − 10.5 kcal/mol in 9PFL, 9PFM, and 8CVN respectively (Table 4). In both X-ray structures its top pose hydrogen-bonded the catalytic Ser138 (2.89 Angstrom in 9PFL, 2.83 Angstrom in 9PFM) and contacted Tyr151 and the lid-hinge Phe185, occupying much the same sub-pocket as the crystallographic inhibitor. In the cryo-electron microscopy structure the top pose instead anchored on the lid-hinge residues Phe185 and Tyr217, both part of the flagged pocket-lining set, while Ser138 and Tyr151 were not reached (Table 5; Figs. 3 to 5). Across all three structures the compound

contacted at least two of the five flagged residues. The lid-hinge Phe185 was the only flagged residue contacted in every structure, at 3.01, 3.12, and 3.16 Angstrom respectively, whereas engagement of the catalytic Ser138 and Tyr151 varied with the receptor conformation. Lys155 was not contacted in any pose, consistent with Lys155 coordinating the cofactor rather than lining the inhibitor space. Interaction profiling with PLIP independently confirmed the Ser138 hydrogen bond and the Phe185 contact as the primary interactions in the X-ray structures, with the full per-residue lists given in the supplementary tables in S1 File.

Table 4
Best predicted docking affinities (kcal/mol).

Structure	Dihydrotanshinone I	Panaxynol	Reference inhibitor (redock)
9PFL	-8.94	-7.19	-13.61
9PFM	-9.56	-7.32	-8.85
8CVN	-10.5	-6.54	-8.82

Table 5
Flagged-residue contacts of the dihydrotanshinone I top pose (minimum heavy-atom distance in Angstrom; values in parentheses lie beyond the 4 Angstrom contact cutoff and are not counted as contacts).

Structure	Ser138	Tyr151	Lys155	Phe185	Tyr217
9PFL	2.89	3.45	(6.73)	3.01	(4.59)
9PFM	2.83	3.60	(6.74)	3.12	(6.28)
8CVN	(4.23)	(6.93)	(8.82)	3.16	3.52

3.4. Comparison with the comparator compound

Panaxynol also docked into the same pocket in all three structures but with consistently weaker predicted affinities than dihydrotanshinone I, at -7.19, -7.32, and − 6.54 kcal/mol (Table 4). It contacted Ser138, Tyr151, and Phe185 in all three structures, and reached Tyr217 in 9PFL and 8CVN at 3.73 and 3.63 Angstrom, while in 9PFM Tyr217 lay 5.71 Angstrom from the ligand and was not contacted. The broader contact set is consistent with its long lipophilic chain running further down the hydrophobic channel than the compact scaffold of dihydrotanshinone I. Panaxynol has been reported to act as a noncompetitive inhibitor of 15-PGDH (Fujimoto et al., 1998), which would imply a binding site distinct from the orthosteric substrate pocket modelled here, so its weaker score in this pocket is not read as evidence against its reported activity. It is treated as a mechanistically distinct comparator, not as a positive control for the orthosteric site.

3.5. Interaction pattern of the reference inhibitor

The redocked crystallographic inhibitor in 9PFL gave a reference interaction pattern against which the docked compounds could be compared (Table 6). It formed hydrogen bonds with Ser138 and Tyr151, pi-stacking with Phe185 and Tyr217, and a halogen bond from one fluorine to the backbone of Ile190, together recovering four of the five flagged residues. The poses of dihydrotanshinone I reproduce a subset of these anchoring contacts in every structure, which is the basis for describing it as engaging the same inhibitor-binding region as the native ligand.

Table 6
Key interactions of the redocked reference inhibitor in 9PFL.

Residue	Interaction type	Note
Ser138	Hydrogen bond	Catalytic residue
Tyr151	Hydrogen bond	Catalytic residue
Phe185	Pi-stacking	Lid hinge
Tyr217	Pi-stacking	Lid hinge
Ile190	Halogen bond	Backbone, from a ligand fluorine

3.6. Cross-conformation consistency

Although dihydrotanshinone I bound favourably in every structure, its top-ranked pose was only partly conserved across the ensemble once the receptors were superposed (Table 7). The two X-ray structures agreed closely on location, with a centroid-to-centroid distance of 1.48 Angstrom between 9PFL and 9PFM, though the compact scaffold was rotated enough to give a larger heavy-atom RMSD of 5.95 Angstrom. The cryo-electron microscopy pose sat at a distinguishably different position, 6 to 7 Angstrom away by centroid and 7 to 9 Angstrom by heavy-atom RMSD. Within each individual structure the docking was well converged, so this divergence is between the receptor structures and not an artefact of poor convergence within a single run. Taken together, dihydrotanshinone I consistently occupies the 15-PGDH inhibitor pocket, but its top pose in 8CVN is a distinct predicted binding mode associated with that receptor conformation, and a single rigid binding orientation across the ensemble is not established by docking alone.

Table 7
Pairwise comparison of the dihydrotanshinone I top poses after backbone superposition.

Pair	Heavy-atom RMSD (Angstrom)	Centroid distance (Angstrom)
9PFL vs 9PFM	5.95	1.48
9PFL vs 8CVN	9.11	7.17
9PFM vs 8CVN	7.37	6.32

3.7. Reproducibility across random seeds

Across fifteen independent random seeds, the top-ranked pose of dihydrotanshinone I was highly reproducible in every structure (Table 8). All fifteen seeds converged to the same pose cluster within 2 Angstrom in each case, with maximum pairwise heavy-atom RMSDs of only 0.10, 0.12, and 0.18 Angstrom in 9PFL, 9PFM, and 8CVN respectively, and best affinities varying by less than 0.06 kcal/mol. The consensus pose lay within 0.03 to 0.09 Angstrom of the originally reported top pose in each structure, and the flagged contacts, Ser138, Tyr151, and Phe185 in the X-ray structures and Phe185 and Tyr217 in the cryo-electron microscopy structure, were preserved in every seed. The best-scoring pose is therefore the dominant, reproducible docking solution, not an isolated high-scoring outlier.

Table 8
Seed robustness of the dihydrotanshinone I top pose across fifteen random seeds.

Structure	Affinity mean ± SD (kcal/mol)	Max pairwise RMSD (Angstrom)	Seeds in dominant cluster	Consensus vs reported (Angstrom)
9PFL	-8.93 ± 0.015	0.10	15 of 15	0.026
9PFM	-9.56 ± 0.013	0.12	15 of 15	0.044
8CVN	-10.52 ± 0.015	0.18	15 of 15	0.092

3.8. Scoring-function dependence of the predicted affinities

To test whether the score ranking depends on the choice of scoring function, the top-ranked pose of each ligand in each receptor was rescored without re-docking, under both the default Vina function and Vinardo (Quiroga & Villarreal, 2016), and the Vina score was decomposed into its intermolecular and torsional components using the program's own output (Table S16 in S1 File). The Vina totals reproduced the values obtained during docking to within 0.01 kcal/mol, on a different operating system and with a separately obtained binary of the same version.

The decomposition shows that the co-crystallised inhibitor makes the stronger protein contacts in every receptor. Its intermolecular energy exceeds that of dihydrotanshinone I by 6.26 kcal/mol in 9PFL, 2.91 kcal/mol in 9PFM and 1.93 kcal/mol in 8CVN. Dihydrotanshinone I nonetheless attains the more favourable total score in 9PFM and 8CVN because it has no rotatable bonds and therefore incurs no torsional penalty, whereas the SW-series inhibitor has eight and is penalised by 3.6 kcal/mol. The same effect separates dihydrotanshinone I from panaxynol, whose intermolecular energy is the more favourable of the two in all three receptors, by 2.66, 2.25 and 0.05 kcal/mol, and whose weaker total score follows from the 4.0 to 4.5 kcal/mol penalty carried by its eleven rotatable bonds. This is consistent with the broader contact set observed for panaxynol in Section 3.4. The reported affinities therefore reflect ligand rigidity as much as complementarity, and should not be read as a prediction that dihydrotanshinone I binds more tightly than a compound of established sub-nanomolar potency. Ligand efficiency offers a more comparable measure across ligands of different size: 0.43 to 0.50 kcal/mol per heavy atom for dihydrotanshinone I, 0.44 for the 9PFL inhibitor and 0.32 for the SW-series inhibitor.

Under Vinardo the ordering within each receptor is unchanged, so the ranking is not an artefact of a single scoring function. Because the poses were generated by the Vina search and held fixed, this test asks whether the ranking survives a change of scoring function, not whether Vinardo would have located the same poses.

3.9. Molecular dynamics of the docked complexes

All nine trajectories completed 100 ns without instability. Temperature held at 300.0 K, density at 1029 to 1032 kg per cubic metre, and potential energy and box volume drifted by less than 0.05 percent of their means over the full production run in every replica, with no constraint failures anywhere. Two checks specified before the simulations were run were also satisfied in all nine trajectories: the cofactor amide bond that had been flagged as stiff for a 2 fs timestep held a mean length of 1.228 Angstrom against a parameter equilibrium of 1.230 Angstrom, with normal thermal fluctuation and no drift, and the ligand retained its internal geometry, with heavy-atom internal RMSD of 0.23 to 0.37 Angstrom and no loss of quinone-ring planarity, indicating no instability attributable to the ligand parameterisation under the simulated conditions.

Dihydrotanshinone I remained in continuous contact with the protein for the entire 100 ns in every one of the nine trajectories, the minimum ligand-to-protein distance never exceeding 4.5 Angstrom in any frame (Table 9); assignment of the ligand to the inhibitor-site region is supported by the residue-level contacts and the ligand RMSD reported below. The three systems nevertheless differed markedly and reproducibly in how far the ligand moved from its docked pose. In 9PFL it barely moved, with ligand RMSD of 0.69 to 0.98 Angstrom across the three replicas; in 9PFM it settled at an intermediate 1.29 to 1.92 Angstrom; and in 8CVN it moved substantially, at 4.64 to 7.49 Angstrom. This ordering was identical in all three replicas of each system, so the relative dynamic persistence of the three docked poses over the simulated timescale is itself a reproducible result.

Table 9
Molecular dynamics simulations performed and ligand positional persistence. Values are given for each of the three replicas.

System	Atoms	Ligand RMSD, three replicas (Angstrom)	Minimum ligand-protein distance (Angstrom)	Frames with minimum ligand-protein distance above 4.5 Angstrom
9PFL	32,448	0.98, 0.69, 0.85	2.87 to 3.03	0 of 30,003
9PFM	36,016	1.92, 1.29, 1.46	3.00 to 3.10	0 of 30,003
8CVN	34,694	7.49, 4.64, 5.86	3.06 to 3.14	0 of 30,003

Contact occupancies over the trajectories are given in Table 10. Two results are unambiguous. Phe185 was in contact for 94.6 to 100 percent of frames in all nine trajectories, making it the only flagged residue engaged essentially continuously in every system and every replica, which independently corroborates the docking finding that Phe185 is the single conserved contact across the ensemble. Conversely, Lys155 was never contacted in any frame of any trajectory, an occupancy of exactly zero in

all nine runs, consistent with its cofactor-coordinating role rather than a role in lining the inhibitor pocket. Tyr217, which the docking predicted as a contact only in 8CVN, was in fact engaged for 67.6 to 92.4 percent of frames in the two X-ray systems as well, so this interaction is formed under dynamics but is not visible in a rigid docked pose.

Table 10
Occupancy of the flagged residues over the molecular dynamics trajectories (percentage of frames within 4 Angstrom, computed over the full production run before any equilibration discard), given for each of the three replicas.

Residue	9PFL	9PFM	8CVN
Ser138	99.8, 98.4, 89.6	83.0, 79.8, 78.7	45.6, 1.9, 3.0
Tyr151	72.7, 62.3, 29.0	97.0, 95.0, 93.4	45.7, 0.2, 0.0
Lys155	0.0, 0.0, 0.0	0.0, 0.0, 0.0	0.0, 0.0, 0.0
Phe185	100.0, 100.0, 100.0	99.6, 100.0, 100.0	98.3, 94.6, 97.4
Tyr217	84.2, 88.9, 81.1	84.2, 67.6, 92.4	98.5, 100.0, 100.0
Ser138 hydrogen bond	55.4, 41.8, 9.1	3.8, 16.1, 2.0	4.5, 0.0, 0.0

Two further results require care in how they are stated. The Ser138 contact was maintained at high occupancy in 9PFL by the distance criterion, but when assessed with proper hydrogen-bond geometry its occupancy varied more than sixfold between replicas, from 55.4 to 41.8 to 9.1 percent (Table 10). A hydrogen bond is therefore present in all three replicas but its persistence is highly variable, and reporting any single one of those values would misrepresent the interaction. In 8CVN, the ligand in one replica relocated within the pocket after about 60 ns and settled into a position 1.40 Angstrom from the 9PFL docked pose, taking on that structure's contact pattern; the other two replicas showed no such transition and never approached the 9PFL pose, fluctuating between roughly 7.8 and 10.7 Angstrom over the run and ending at 8.6 to 8.8 Angstrom. That relocation is therefore a single-trajectory event rather than a general property of the system, and is reported as such.

Applying the same cross-fitting analysis to the X-ray systems provides the calibration against which those numbers should be read. The 9PFL ligand stayed 0.97 to 1.36 Angstrom from its own docked pose in all three replicas, and the 9PFM ligand held steady at 5.75 to 5.90 Angstrom from the 9PFL pose in all three of its replicas, with no drift toward it. The docked poses of the two X-ray structures are therefore genuinely distinct from one another and each is stable in its own receptor conformation, rather than converging on a common orientation once receptor flexibility is allowed.

Because the equilibration discard windows were chosen by inspection of each trajectory's own backbone deviation, the occupancies in Table 10 were recomputed at discard windows of 0, 10, 20, 30 and 50 ns to test whether any conclusion depends on that choice. The three principal results do not. Phe185 remained above 94 percent at every window in all nine trajectories, with a lowest single value of 94.7 percent; Lys155 remained exactly zero in all forty-five values; and Tyr217 remained above 65 percent at

every window in all six X-ray trajectories, with a lowest single value of 67.8 percent. Lys155 did not vary at all, and Phe185 varied by at most 4.3 percentage points across the full range of windows in any run while never falling below 94 percent.

Ser138, Tyr151 and the Ser138 hydrogen bond are more sensitive to the window, and in three trajectories the variation is directional, not noise. In the third 9PFL replica the Tyr151 occupancy falls steadily from 29.1 to 1.2 percent and the Ser138 hydrogen bond from 9.1 to 0.04 percent as the window advances, indicating a progressive loss of the polar anchor over the run. In the first 8CVN replica the Ser138 and Tyr151 occupancies rise from about 46 percent to between 75 and 79 percent, which reflects the relocation described above, and in the first 9PFM replica the Tyr217 occupancy rises from 84.3 to 97.6 percent, consistent with that system's continued backbone drift. For these residues a single figure summarises a changing quantity, and the values in Table 10 should be read as run averages rather than as steady-state occupancies. A further limit on precision applies throughout: occupancy is defined by a hard 4 Angstrom cutoff and roughly 7 percent of frames lie within half a picometre of that threshold, so occupancies computed through independently written analysis pipelines agree to approximately 0.3 percentage points, not exactly.

Fluctuation analysis distinguished the two lid residues that docking had treated together. Phe185 fluctuated less than the protein average in all nine trajectories, while Tyr217 fluctuated more than the average in all nine. Phe185 therefore behaves as a persistent and relatively rigid contact rather than a mobile element, and the mobility associated with the lid is carried by Tyr217. Table 11 summarises which observations reproduce across replicas and which do not.

Table 11
Replicate agreement across the nine trajectories.

Observation	Replicates showing it
Ligand remains in continuous contact with the protein throughout	9 of 9
Phe185 occupancy of 94.6 percent or above	9 of 9
Lys155 never contacted	9 of 9
Phe185 fluctuates less than the protein average	9 of 9
Tyr217 fluctuates more than the protein average	9 of 9
Tyr217 contact above 65 percent in the X-ray systems	6 of 6
Relative ligand RMSD from the docked pose 9PFL < 9PFM < 8CVN	3 of 3 per system
Ser138 hydrogen bond above 50 percent in 9PFL	1 of 3
8CVN ligand relocating to the 9PFL pose	1 of 3

4. Discussion

This study asked whether dihydrotanshinone I, a defined natural compound not previously examined against 15-PGDH, can occupy the enzyme's inhibitor pocket. The answer from validated docking is that dihydrotanshinone I can be accommodated within the known 15-PGDH inhibitor pocket, in a pose that scores favourably and recurs consistently across independent docking runs. In all three inhibitor-bound structures the compound docked into the pocket with favourable predicted affinity and engaged the mechanistically important residues, hydrogen bonding the catalytic Ser138 and contacting Tyr151 and the lid-hinge Phe185 in the X-ray structures and anchoring on Phe185 and Tyr217 in the cryo-electron microscopy structure. The redocking validation, with heavy-atom RMSDs of 0.38 to 1.46 Angstrom, and the seed-robustness analysis, in which fifteen independent seeds converged to the same pose in every structure, together give confidence that this is a real and reproducible docking result, not an artefact of the setup or the random seed.

The predicted binding mode is consistent with the known determinants of inhibitor recognition in 15-PGDH. Ser138 and Tyr151 are two members of the catalytic triad (Zhou et al., 2001), and Phe185 and Tyr217 are the experimentally defined lid hinges that potent inhibitors exploit to trap the closed conformation (Huang et al., 2023). Prior computational work on the synthetic inhibitor SW033291 reached the same set of residues, concluding that inhibitors of 15-PGDH engage Ser138, Tyr151, and Phe185 in the cofactor complex (Mallipeddi et al., 2021). That the residues contacted by a natural diterpenoid quinone coincide with those independently identified for a designed synthetic inhibitor is meaningful corroboration, and it positions the present work as extending to a defined natural compound the kind of structure-based analysis previously reported only for synthetic inhibitors.

The result that requires care is the pose conservation. While the location and the key contacts were consistent, the precise top-pose orientation was only partly conserved across the ensemble, with the two X-ray poses agreeing on location but the cryo-electron microscopy pose displaced. Because the three receptor conformations are globally very similar and dihydrotanshinone I is small relative to the pocket, this may reflect a scoring landscape in which several similar-scoring orientations are available, so a single binding mode is not resolved. The distinct top pose in the single cryo-electron microscopy structure warrants the same caution: with only one such structure available, its difference from the two X-ray poses could reflect local pocket geometry, the receptor conformational state, the different cofactor redox state (8CVN carries NADH at net charge − 2 while both X-ray receptors carry NAD at net charge − 1, immediately adjacent to the pocket), differences between X-ray and cryo-electron microscopy models, or docking uncertainty, and these cannot be separated in the present design. It is therefore described as a predicted binding mode associated with the 8CVN conformation rather than as a biologically distinct one. Docking alone cannot decide which orientation is physically preferred, which is why the molecular dynamics reported in Section 3.9 was carried out to test whether this alternative pose remains stable.

The comparator strengthens rather than weakens the interpretation. Panaxynol, the best-characterised botanical inhibitor of 15-PGDH, docked more weakly into the orthosteric pocket, consistent with its reported noncompetitive mechanism and a binding site distinct from the orthosteric pocket (Fujimoto et al., 1998). Its weaker orthosteric score is therefore expected and does not contradict its known activity,

and dihydrotanshinone I, which docks cleanly into the pocket the study concerns, is the more suitable orthosteric-pocket candidate of the two.

Molecular dynamics was carried out to examine two questions left open by docking, and it addresses both within the limits set out below. The first was whether the docked pose persists once the receptor is free to move. It is: the ligand remained in contact with the protein for the whole of every one of nine 100 ns trajectories, and retained contacts with the residues that line the inhibitor site, and in the primary X-ray structure it barely moved from its docked position. The second was whether the differing orientations across the ensemble reflect a genuine difference between conformations or an artefact of rigid-receptor docking. Under dynamics the poses remained distinct, with the 9PFM ligand holding a constant separation from the 9PFL pose in all three of its replicas rather than drifting toward it, so the conclusion drawn from docking, that a single rigid binding orientation is not established across the ensemble, is supported rather than overturned. In one 8CVN replica the ligand did relocate to within 1.40 Angstrom of the 9PFL pose after 60 ns, which would have been a striking result had it recurred; it did not recur in the other two replicas, and it is reported here as a single-trajectory observation precisely because triplicate simulation is what distinguishes such an event from a general property.

The simulations also sharpen two specific points. Phe185 emerges as the anchor of this interaction in a stronger sense than docking alone could show: it is contacted in essentially every frame of every trajectory, and it fluctuates less than the protein average in all nine runs, so it behaves as a persistent and relatively rigid contact within the lid region. On this evidence the greater local mobility within the lid region is associated with Tyr217, which fluctuates more than average in all nine trajectories, rather than by the two hinge residues equally. Tyr217 also forms a persistent contact in the X-ray systems that the docked poses did not register. In 9PFL the docked pose placed it at 4.59 Angstrom, just outside the 4 Angstrom contact definition (Table 5), so this is a contact the static pose came close to making and that ordinary thermal motion then sustains for most frames. The same applies to Ser138 in 8CVN at 4.23 Angstrom. This is the kind of near-threshold interaction a rigid single-pose calculation is expected to miss. Conversely, the hydrogen bond to the catalytic Ser138, which appeared well defined in the docked poses, proves highly variable under dynamics, ranging from 9 to 55 percent occupancy across replicas of the same system. Both observations point the same way: docking identifies where the compound sits and which residues line that site, but the persistence of individual interactions is not something a single static pose can establish.

Several limitations bound these conclusions. The receptors were treated as rigid during docking, so the docking itself cannot capture the induced-fit lid closure that accompanies inhibitor binding in this enzyme, and the ensemble sampled only closely related inhibitor-bound conformations, not the open state. The comparator panaxynol carries eleven rotatable bonds, and its top-ranked pose proved less well determined than its score: re-running the same inputs, seed and search parameters on a different operating system returned affinities within 0.54 kcal/mol but, in 9PFM and 8CVN, a top pose displaced by around 7 Angstrom with a substantially different contact set. The panaxynol contacts reported here should therefore be read as one low-energy arrangement rather than a converged prediction. The

dihydrotanshinone I poses and the redocking validations reproduced to within 0.04 Angstrom under the same test. Most importantly, neither the docking nor the simulations establish enzyme inhibition. The predicted affinities are relative estimates rather than measured constants, and the simulations describe geometric persistence, not binding strength. Experimental enzyme assays remain the necessary test, and for this scaffold they should be accompanied by appropriate counter-screens. Dihydrotanshinone I is an ortho-quinone, a class associated with redox cycling, reactivity toward thiols and assay interference, and it has been reported as a binder against a range of unrelated targets. Activity in a single biochemical assay would therefore not by itself establish specific engagement of 15-PGDH.

The simulations carry their own limits. Each trajectory ran for 100 ns, giving 300 ns per system, which is short relative to the timescales on which a ligand might sample alternative orientations within a pocket. In the 9PFM system the backbone root mean square deviation continued to drift in all three replicas without reaching a clean plateau, so 100 ns may be shorter than that system's relaxation time. No binding free energy was calculated, so the simulations provide no thermodynamic ranking of binding affinity; they characterise dynamic persistence and interaction occupancy instead. Each system was simulated as a single protomer, so the dimer interface of the physiological homodimer was solvent-exposed throughout; this is a plausible contributor to the continued backbone drift seen in 9PFM. Each system was simulated from a single docked starting pose, so competing orientations within the same pocket were not sampled from alternative starting points, and the three replicas of each system share one solvated build and differ only in their initial velocities, not in ion placement or solvent configuration. In the ligand parameterisation, four torsions at the ring-fusion bonds were assigned by analogy, with penalty scores between 223 and 319, although all bond, angle and non-bonded terms matched the parent force field directly and the ligand's internal geometry remained stable throughout, with internal root mean square deviations of 0.23 to 0.37 Angstrom and a planar quinone in all nine runs. The cofactor parameters were developed for earlier AMBER force fields and were used here with ff14SB, and two nicotinamide carbon-hydrogen improper terms were absent from that set. The affected centres remained planar on average, with a mean absolute out-of-plane deviation of 9.2 degrees against 5.5 degrees for parameterised aromatic centres in the same trajectory, and both lie remote from the ligand site. The same cofactor set assigns an unusually stiff force constant to the nicotinamide amide carbonyl, 860 kcal per mole per square Angstrom against the 570 to 590 typical of AMBER-family carbonyls, which implies a stretch frequency well above the normal amide I range. This is a property of the original parameterisation, not of the present pipeline, and it was the reason this bond was monitored throughout production, where it held at its equilibrium length in all nine trajectories. Finally, contact occupancy is defined by a hard 4 Angstrom cutoff, and because a substantial fraction of frames sit close to that threshold, occupancies are reproducible to approximately 0.3 percentage points between independent analysis pipelines.

5. Conclusion

Using a protocol validated by redocking in every receptor and shown to be reproducible across random seeds, dihydrotanshinone I was found to dock favourably and consistently into the inhibitor pocket of

human 15-PGDH across three inhibitor-bound structures, engaging the catalytic and lid-hinge residues used by known inhibitors. Its top-pose orientation is not fully conserved across the ensemble, so a single rigid binding mode is not yet established, but the combined docking and simulation analyses support persistent association of the compound with the inhibitor-site region. Dihydrotanshinone I is therefore identified as a novel, mechanistically plausible natural-compound candidate for the 15-PGDH inhibitor pocket. All predicted binding is reported as binding potential and mechanistic plausibility, not as proven inhibition.

Triplicate 100 ns molecular dynamics simulations of all three complexes, nine trajectories in total, support and refine this picture. The compound remained in continuous contact with the protein throughout every trajectory and retained its contacts with the inhibitor-site residues; Phe185 was contacted in essentially every frame of all nine runs while Lys155 was contacted in none, corroborating both the conserved-contact finding and the cofactor-coordination interpretation; and the three docked poses remained largely distinct under receptor flexibility, with one 8CVN replica of nine relocating toward the 9PFL pose, upholding the conclusion that a single rigid binding orientation is not established. The simulations further show that Phe185 acts as a persistent and relatively rigid contact while Tyr217 carries the lid mobility and forms a persistent contact that the docked pose placed just outside the contact cutoff, and that the hydrogen bond to Ser138 is real but variable. Experimental enzyme assays remain the necessary next step to test for inhibition.

Declarations

Data Availability

All input structures, force-field parameters, topology and run-input files, build scripts, analysis scripts and analysis outputs supporting this study are archived at Zenodo (DOI: https://doi.org/10.5281/zenodo.21945974). The record contains the three docked starting complexes, the prepared receptor, ligand and cofactor coordinates, the ligand and cofactor parameter files, the seven GROMACS run-input files, the tleap build scripts, the docking inputs and outputs, and the per-trajectory analysis outputs. It also contains an independent reproduction of all nine docking runs, executed from byte-identical inputs on a different operating system and a different compiled binary. The nine production trajectories are included in the same record as individual uncompressed files, so that a single trajectory can be retrieved without downloading the complete set. No restrictions apply to any of these materials.

References

1. Abraham, M. J., Murtola, T., Schulz, R., Pall, S., Smith, J. C., Hess, B., & Lindahl, E. (2015). GROMACS: High performance molecular simulations through multi-level parallelism from laptops to supercomputers. *SoftwareX, 1-2*, 19-25. https://doi.org/10.1016/j.softx.2015.06.001
2. Ahmad, S. S., Lim, J. H., Choi, I., & Lee, E. J. (2024). Biocomputational screening of natural compounds targeting 15-hydroxyprostaglandin dehydrogenase to improve skeletal muscle during

aging. *Molecular Diversity, 28*(6), 4425-4439. https://doi.org/10.1007/s11030-024-10825-9

3. Bernetti, M., & Bussi, G. (2020). Pressure control using stochastic cell rescaling. *The Journal of Chemical Physics, 153*(11), 114107. https://doi.org/10.1063/5.0020514
4. Burley, S. K., Bhikadiya, C., Bi, C., Bittrich, S., Chao, H., Chen, L., Craig, P. A., Crichlow, G. V., Dalenberg, K., Duarte, J. M., Dutta, S., Fayazi, M., Feng, Z., Flatt, J. W., Ganesan, S., Ghosh, S., Goodsell, D. S., Green, R. K., Guranovic, V., ... Zardecki, C. (2023). RCSB Protein Data Bank (RCSB.org): Delivery of experimentally-determined PDB structures alongside one million computed structure models of proteins from artificial intelligence/machine learning. *Nucleic Acids Research, 51*(D1), D488-D508. https://doi.org/10.1093/nar/gkac1077
5. Bussi, G., Donadio, D., & Parrinello, M. (2007). Canonical sampling through velocity rescaling. *The Journal of Chemical Physics, 126*(1), 014101. https://doi.org/10.1063/1.2408420
6. Case, D. A., Aktulga, H. M., Belfon, K., Cerutti, D. S., Cisneros, G. A., Cruzeiro, V. W. D., Forouzesh, N., Giese, T. J., Götz, A. W., Gohlke, H., Izadi, S., Kasavajhala, K., Kaymak, M. C., King, E., Kurtzman, T., Lee, T.-S., Li, P., Liu, J., Luchko, T., ... Merz, K. M. (2023). AmberTools. *Journal of Chemical Information and Modeling, 63*(20), 6183-6191. https://doi.org/10.1021/acs.jcim.3c01153
7. Cock, P. J. A., Antao, T., Chang, J. T., Chapman, B. A., Cox, C. J., Dalke, A., Friedberg, I., Hamelryck, T., Kauff, F., Wilczynski, B., & de Hoon, M. J. L. (2009). Biopython: Freely available Python tools for computational molecular biology and bioinformatics. *Bioinformatics, 25*(11), 1422-1423. https://doi.org/10.1093/bioinformatics/btp163
8. Cui, S., Chen, S., Wu, Q., Chen, T., & Li, S. (2020). A network pharmacology approach to investigate the anti-inflammatory mechanism of effective ingredients from Salvia miltiorrhiza. *International Immunopharmacology, 81*, 106040. https://doi.org/10.1016/j.intimp.2019.106040
9. Darden, T., York, D., & Pedersen, L. (1993). Particle mesh Ewald: An N log(N) method for Ewald sums in large systems. *The Journal of Chemical Physics, 98*(12), 10089-10092. https://doi.org/10.1063/1.464397
10. Dodda, L. S., Campos, S., Ciccone, D., Carreiro, S., Leit, S., Brennan, D., Zephyr, J., Jacques-O'Hagan, S., Kumar, S., Kuo, F.-S., Shaik, M. M., Price, D. J., Loh, C., Edmondson, S. D., Tummino, P., & Kaila, N. (2025). Knowledge and structure-based drug design of 15-PGDH inhibitors. *Journal of Medicinal Chemistry, 68*(17), 18436-18462. https://doi.org/10.1021/acs.jmedchem.5c01231
11. Eberhardt, J., Santos-Martins, D., Tillack, A. F., & Forli, S. (2021). AutoDock Vina 1.2.0: New docking methods, expanded force field, and Python bindings. *Journal of Chemical Information and Modeling, 61*(8), 3891-3898. https://doi.org/10.1021/acs.jcim.1c00203
12. Forli Lab. (n.d.). *Meeko: Preparation of small molecules for AutoDock* [Computer software]. GitHub. https://github.com/forlilab/Meeko
13. Fujimoto, Y., Sakuma, S., Komatsu, S., Sato, D., Nishida, H., Xiao, Y. Q., Baba, K., & Fujita, T. (1998). Inhibition of 15-hydroxyprostaglandin dehydrogenase activity in rabbit gastric antral mucosa by panaxynol isolated from oriental medicines. *Journal of Pharmacy and Pharmacology, 50*(9), 1075-1078. https://doi.org/10.1111/j.2042-7158.1998.tb06925.x

14. Gasteiger, J., & Marsili, M. (1980). Iterative partial equalization of orbital electronegativity: A rapid access to atomic charges. *Tetrahedron, 36*(22), 3219-3228. https://doi.org/10.1016/0040-4020(80)80168-2
15. Halgren, T. A. (1996). Merck molecular force field. I. Basis, form, scope, parameterization, and performance of MMFF94. *Journal of Computational Chemistry, 17*(5-6), 490-519. https://doi.org/10.1002/(SICI)1096-987X(199604)17:5/6<490::AID-JCC1>3.0.CO;2-P
16. Hess, B., Bekker, H., Berendsen, H. J. C., & Fraaije, J. G. E. M. (1997). LINCS: A linear constraint solver for molecular simulations. *Journal of Computational Chemistry, 18*(12), 1463-1472. https://doi.org/10.1002/(SICI)1096-987X(199709)18:12<1463::AID-JCC4>3.0.CO;2-H
17. Huang, W., Li, H., Kiselar, J., Fink, S. P., Regmi, S., Day, A., Yuan, Y., Chance, M., Ready, J. M., Markowitz, S. D., & Taylor, D. J. (2023). Small molecule inhibitors of 15-PGDH exploit a physiologic induced-fit closing system. *Nature Communications, 14*, 784. https://doi.org/10.1038/s41467-023-36463-7
18. Jakalian, A., Jack, D. B., & Bayly, C. I. (2002). Fast, efficient generation of high-quality atomic charges. AM1-BCC model: II. Parameterization and validation. *Journal of Computational Chemistry, 23*(16), 1623-1641. https://doi.org/10.1002/jcc.10128
19. Jorgensen, W. L., Chandrasekhar, J., Madura, J. D., Impey, R. W., & Klein, M. L. (1983). Comparison of simple potential functions for simulating liquid water. *The Journal of Chemical Physics, 79*(2), 926-935. https://doi.org/10.1063/1.445869
20. Joung, I. S., & Cheatham, T. E., III. (2008). Determination of alkali and halide monovalent ion parameters for use in explicitly solvated biomolecular simulations. *Journal of Physical Chemistry B, 112*(30), 9020-9041. https://doi.org/10.1021/jp8001614
21. Kabsch, W. (1976). A solution for the best rotation to relate two sets of vectors. *Acta Crystallographica Section A, 32*(5), 922-923. https://doi.org/10.1107/S0567739476001873
22. Kim, S., Chen, J., Cheng, T., Gindulyte, A., He, J., He, S., Li, Q., Shoemaker, B. A., Thiessen, P. A., Yu, B., Zaslavsky, L., Zhang, J., & Bolton, E. E. (2023). PubChem 2023 update. *Nucleic Acids Research, 51*(D1), D1373-D1380. https://doi.org/10.1093/nar/gkac956
23. Landrum, G. (n.d.). *RDKit: Open-source cheminformatics* [Computer software]. https://www.rdkit.org
24. Maier, J. A., Martinez, C., Kasavajhala, K., Wickstrom, L., Hauser, K. E., & Simmerling, C. (2015). ff14SB: Improving the accuracy of protein side chain and backbone parameters from ff99SB. *Journal of Chemical Theory and Computation, 11*(8), 3696-3713. https://doi.org/10.1021/acs.jctc.5b00255
25. Mallipeddi, P. L., Zhang, Y., Li, H., Markowitz, S. D., & Posner, B. (2021). Structural insights into novel 15-prostaglandin dehydrogenase inhibitors. *Molecules, 26*(19), 5903. https://doi.org/10.3390/molecules26195903
26. Niesen, F. H., Schultz, L., Jadhav, A., Bhatia, C., Guo, K., Maloney, D. J., Pilka, E. S., Wang, M., Oppermann, U., Heightman, T. D., & Simeonov, A. (2010). High-affinity inhibitors of human NAD+-

dependent 15-hydroxyprostaglandin dehydrogenase: Mechanisms of inhibition and structure-activity relationships. *PLoS ONE, 5*(11), e13719. https://doi.org/10.1371/journal.pone.0013719

27. O'Boyle, N. M., Banck, M., James, C. A., Morley, C., Vandermeersch, T., & Hutchison, G. R. (2011). Open Babel: An open chemical toolbox. *Journal of Cheminformatics, 3*, 33. https://doi.org/10.1186/1758-2946-3-33
28. Palla, A. R., Ravichandran, M., Wang, Y. X., Alexandrova, L., Yang, A. V., Kraft, P., Holbrook, C. A., Schürch, C. M., Ho, A. T. V., & Blau, H. M. (2021). Inhibition of prostaglandin-degrading enzyme 15-PGDH rejuvenates aged muscle mass and strength. *Science, 371*(6528), eabc8059. https://doi.org/10.1126/science.abc8059
29. Parrinello, M., & Rahman, A. (1981). Polymorphic transitions in single crystals: A new molecular dynamics method. *Journal of Applied Physics, 52*(12), 7182-7190. https://doi.org/10.1063/1.328693
30. Pavelites, J. J., Gao, J., Bash, P. A., & MacKerell, A. D., Jr. (1997). A molecular mechanics force field for NAD+, NADH, and the pyrophosphate groups of nucleotides. *Journal of Computational Chemistry, 18*(2), 221-239. https://doi.org/10.1002/(SICI)1096-987X(19970130)18:2<221::AID-JCC7>3.0.CO;2-X
31. Quiroga, R., & Villarreal, M. A. (2016). Vinardo: A scoring function based on AutoDock Vina improves scoring, docking, and virtual screening. *PLOS ONE, 11*(5), e0155183. https://doi.org/10.1371/journal.pone.0155183
32. Salentin, S., Schreiber, S., Haupt, V. J., Adasme, M. F., & Schroeder, M. (2015). PLIP: Fully automated protein-ligand interaction profiler. *Nucleic Acids Research, 43*(W1), W443-W447. https://doi.org/10.1093/nar/gkv315
33. Schake, P., Bolz, S. N., Linnemann, K., & Schroeder, M. (2025). PLIP 2025: Introducing protein-protein interactions to the protein-ligand interaction profiler. *Nucleic Acids Research, 53*(W1), W463-W465. https://doi.org/10.1093/nar/gkaf361
34. Schrodinger, LLC. (n.d.). *The PyMOL molecular graphics system* (Version 3.2) [Computer software].
35. Sousa da Silva, A. W., & Vranken, W. F. (2012). ACPYPE: AnteChamber PYthon Parser interfacE. *BMC Research Notes, 5*, 367. https://doi.org/10.1186/1756-0500-5-367
36. Trott, O., & Olson, A. J. (2010). AutoDock Vina: Improving the speed and accuracy of docking with a new scoring function, efficient optimization, and multithreading. *Journal of Computational Chemistry, 31*(2), 455-461. https://doi.org/10.1002/jcc.21334
37. Walker, R. C., de Souza, M. M., Mercer, I. P., Gould, I. R., & Klug, D. R. (2002). Large and fast relaxations inside a protein: Calculation and measurement of reorganization energies in alcohol dehydrogenase. *Journal of Physical Chemistry B, 106*(44), 11658-11665. https://doi.org/10.1021/jp0261814
38. Wang, J., Wolf, R. M., Caldwell, J. W., Kollman, P. A., & Case, D. A. (2004). Development and testing of a general amber force field. *Journal of Computational Chemistry, 25*(9), 1157-1174. https://doi.org/10.1002/jcc.20035
39. Wojdyr, M. (2022). GEMMI: A library for structural biology. *Journal of Open Source Software, 7*(73), 4200. https://doi.org/10.21105/joss.04200

40. Yue, J., Hao, D., Wang, Y., Guo, J., Liu, S., Meng, L., & Liu, J. (2024). The multifaceted mechanisms of dihydrotanshinone I in the treatment of tumors. *Biomedicine & Pharmacotherapy, 175*, 116635. https://doi.org/10.1016/j.biopha.2024.116635
41. Zhang, Y., Desai, A., Yang, S. Y., Bae, K. B., Antczak, M. I., Fink, S. P., Tiwari, S., Willis, J. E., Williams, N. S., Dawson, D. M., Wald, D., Chen, W. D., Wang, Z., Kasturi, L., Larusch, G. A., He, L., Cominelli, F., Di Martino, L., Djuric, Z., ... Markowitz, S. D. (2015). Inhibition of the prostaglandin-degrading enzyme 15-PGDH potentiates tissue regeneration. *Science, 348*(6240), aaa2340. https://doi.org/10.1126/science.aaa2340
42. Zhou, H., Yan, F., & Tai, H.-H. (2001). C-Terminal region of human NAD+-dependent 15-hydroxyprostaglandin dehydrogenase is involved in the interaction with prostaglandin substrates. *European Journal of Biochemistry, 268*(12), 3368-3374. https://doi.org/10.1046/j.1432-1327.2001.02218.x

Figures

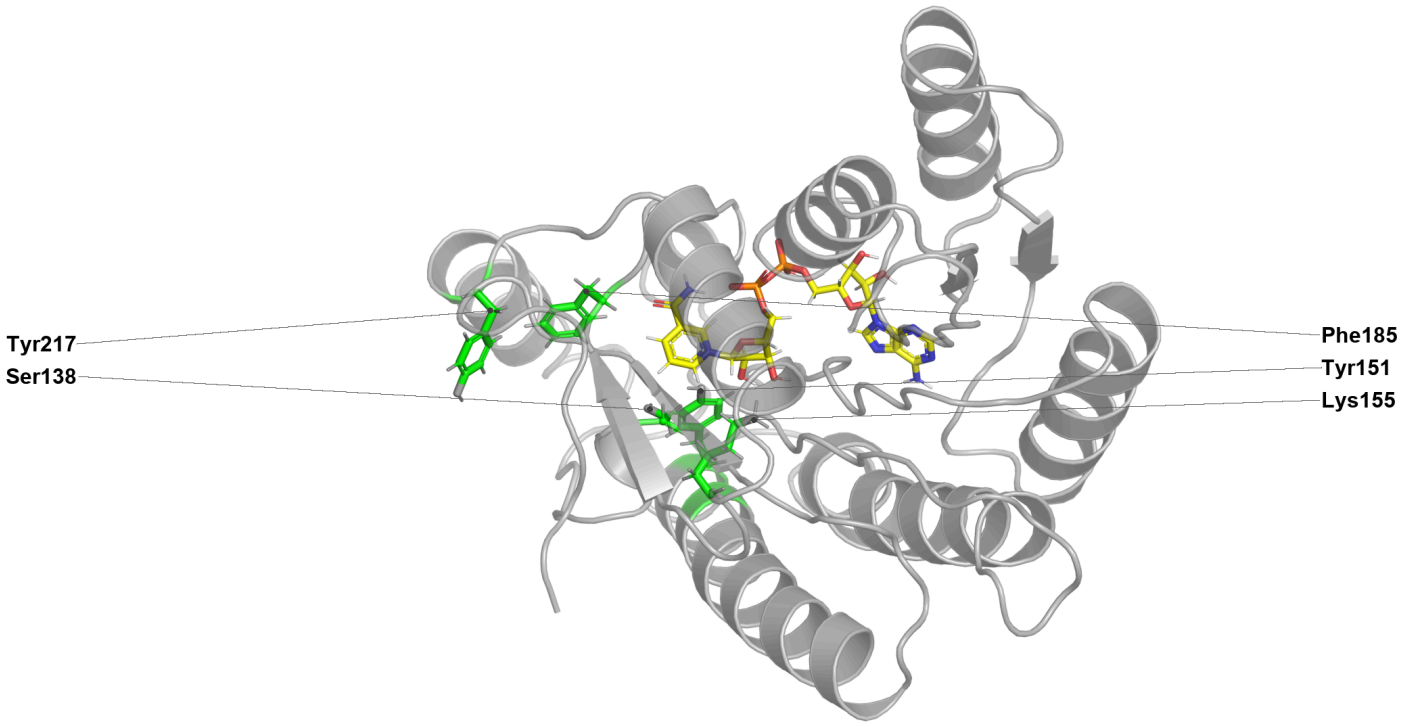


Figure 1

The 15-PGDH inhibitor pocket in 9PFL, with the bound NAD cofactor shown as yellow sticks and the flagged residues Ser138, Tyr151, Lys155, Phe185, and Tyr217 shown as green sticks and labelled.

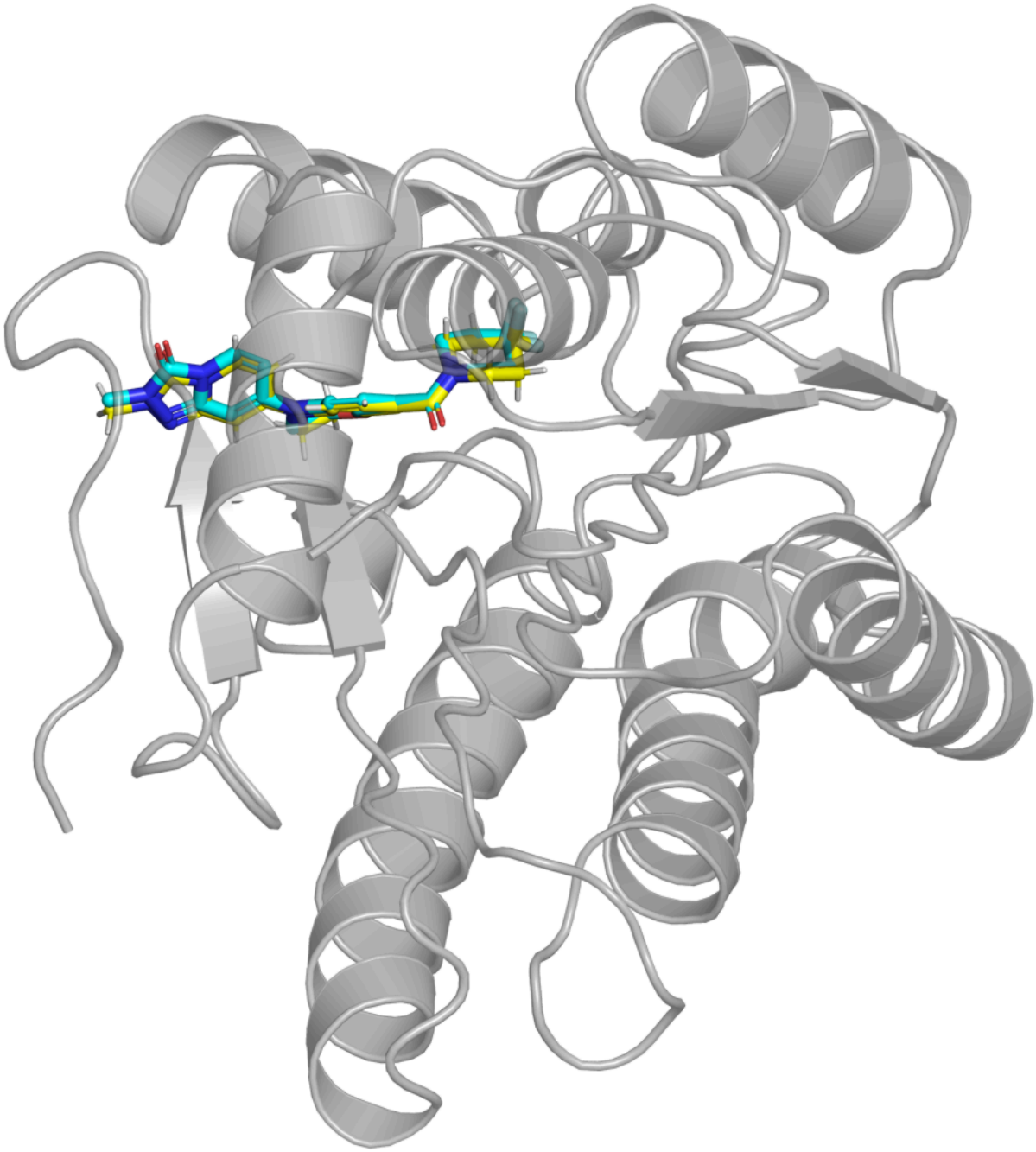


Figure 2

Redocking validation in 9PFL. The crystallographic inhibitor pose (yellow) is overlaid on the top-ranked redocked pose (cyan); heavy-atom RMSD, 0.379 Angstrom.

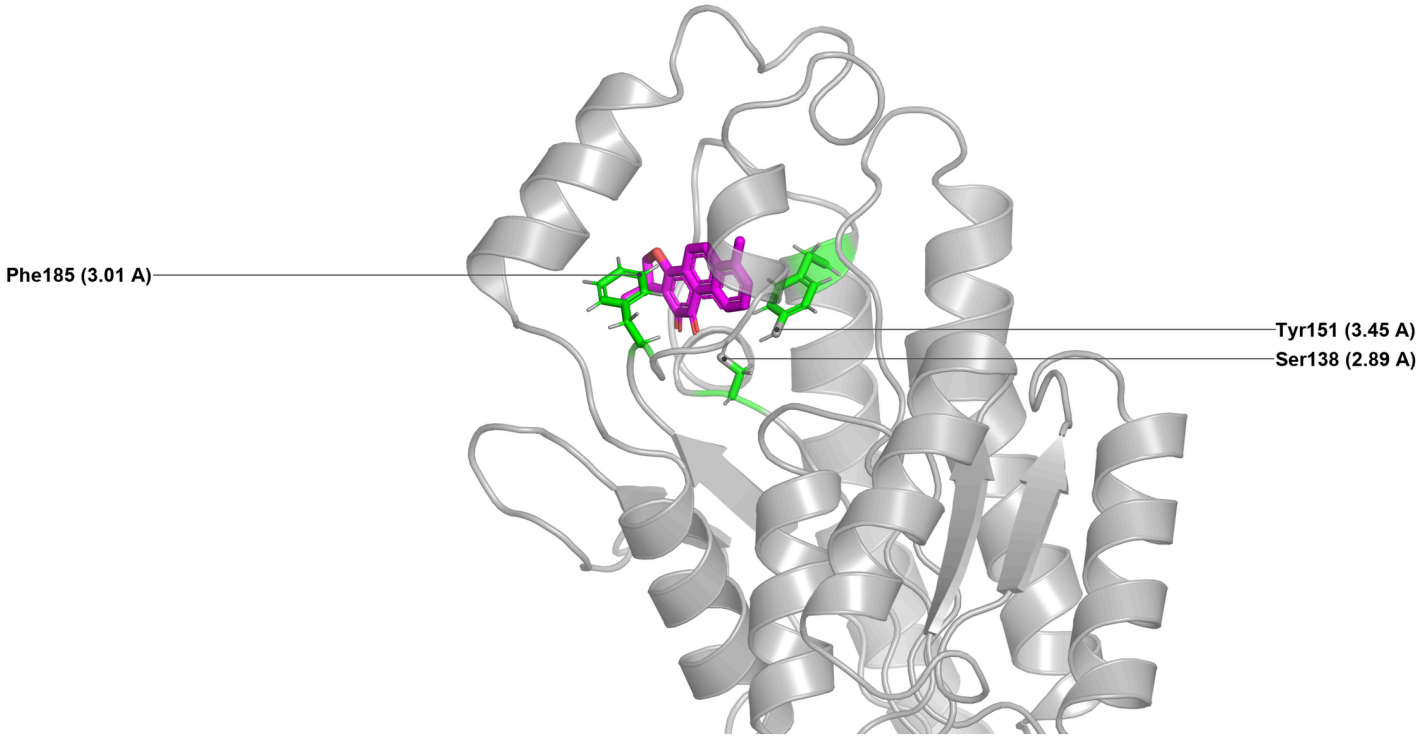


Figure 3

Top-ranked pose of dihydrotanshinone I in 9PFL. Dashed lines mark the contacts to Ser138, Tyr151, and Phe185, with distances as in Table 5.

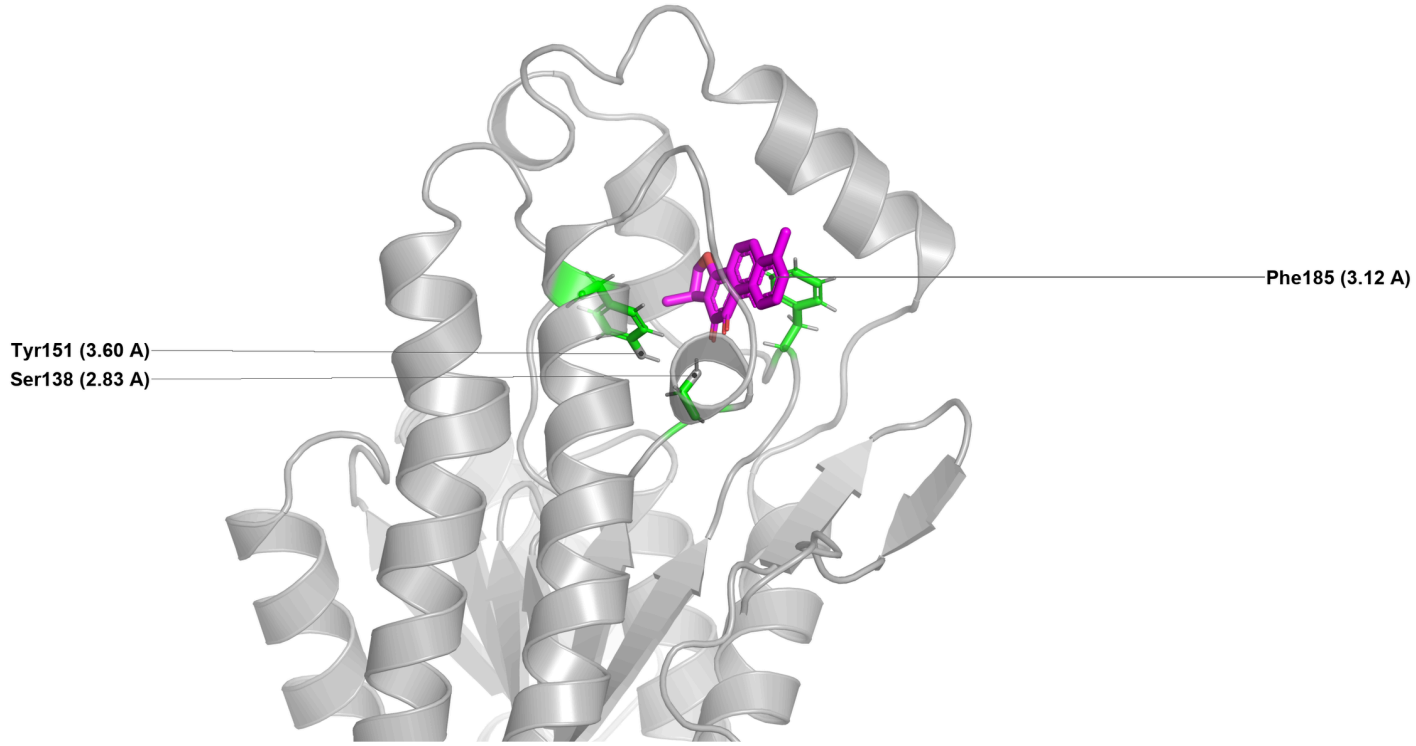


Figure 4

Top-ranked pose of dihydrotanshinone I in 9PFM. Dashed lines mark the contacts to Ser138, Tyr151, and Phe185, with distances as in Table 5.

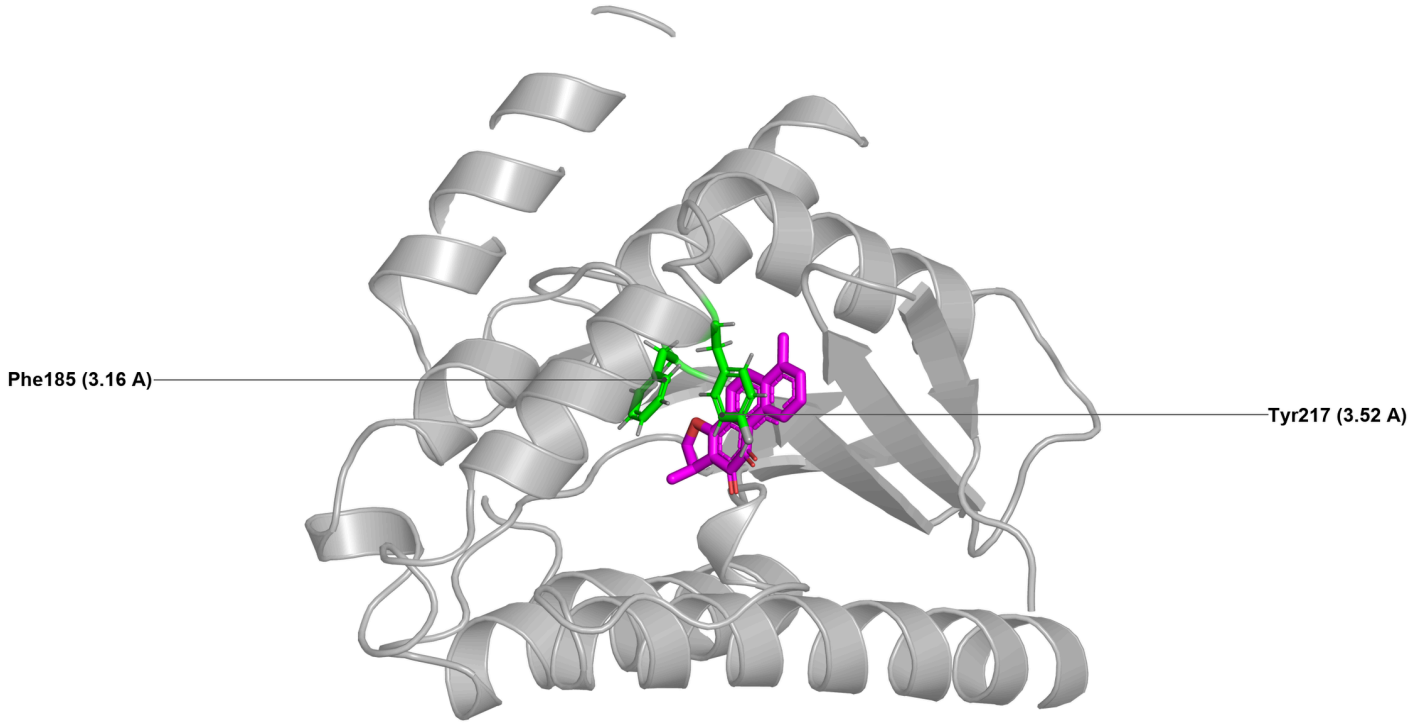


Figure 5

Top-ranked pose of dihydrotanshinone I in 8CVN. Dashed lines mark the contacts to Phe185 and Tyr217, with distances as in Table 5. Ser138 and Tyr151 are not contacted in this conformation.

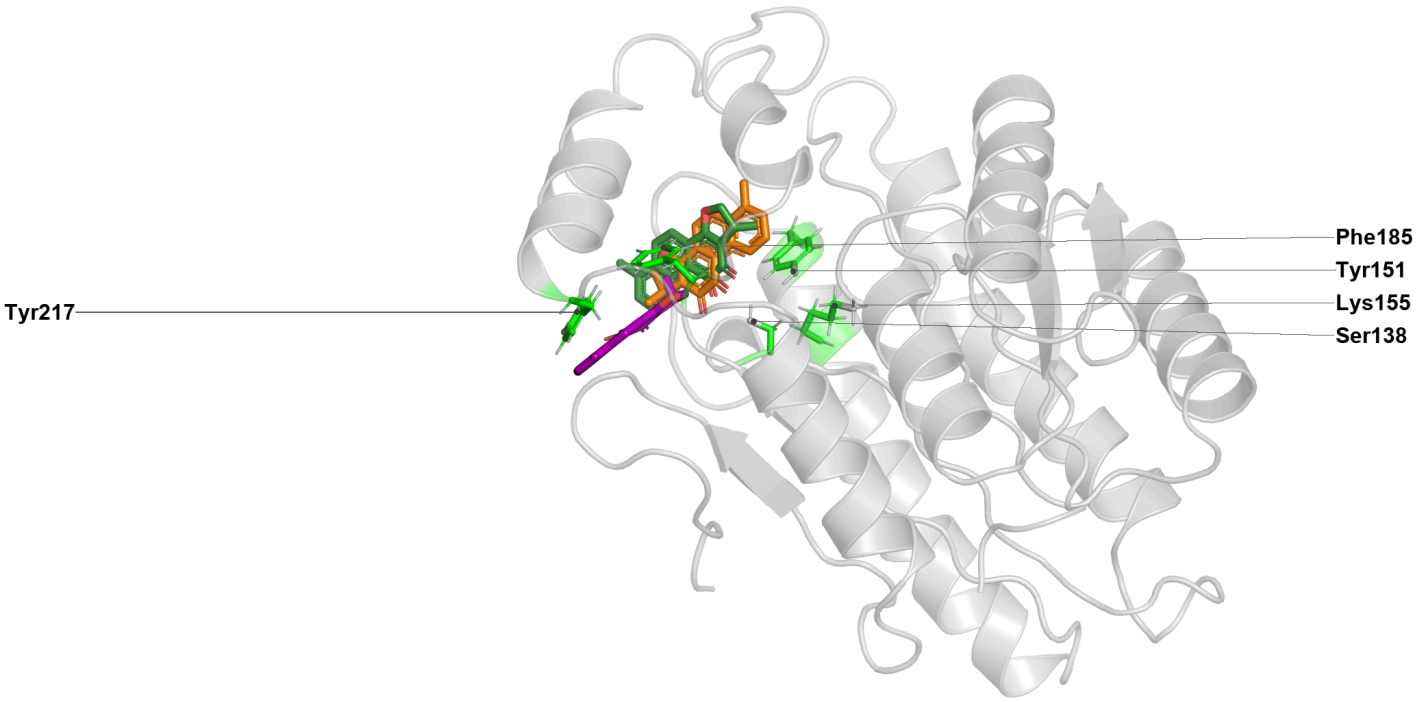


Figure 6

The three top-ranked dihydrotanshinone I poses after superposing 9PFM and 8CVN onto 9PFL. Orange, 9PFL; green, 9PFM; purple, 8CVN. The two X-ray poses occupy nearly the same location; the cryo-EM pose is shifted.

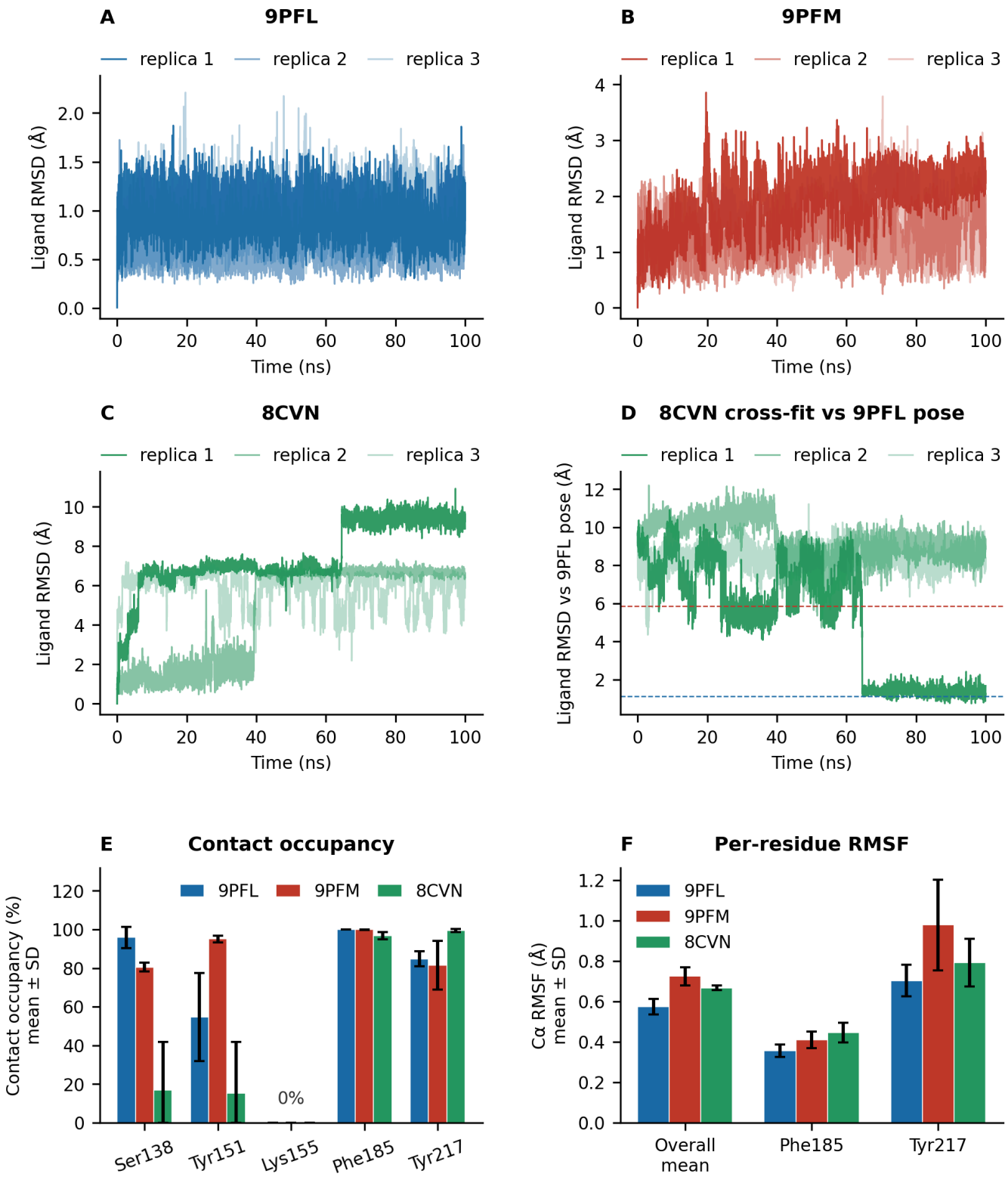


Figure 7

Molecular dynamics of the three docked complexes over three 100 ns replicas each. (A to C) Ligand heavy-atom RMSD from the docked pose for 9PFL, 9PFM and 8CVN, computed after least-squares fitting on protein backbone atoms; all three replicas per system are shown, shaded dark to light for replicas 1 to 3. (D) Distance of the 8CVN ligand from the 9PFL docked pose after per-frame superposition on the 255 shared C-alpha atoms, showing the relocation seen in one replica only; the dashed blue line marks the 9PFL self-

reference at a replicate mean of 1.1 Angstrom and the dashed red line the 9PFM reference at a replicate mean of 5.8 Angstrom. (E) Contact occupancy of the flagged residues over the full production run, measured as the percentage of frames with a minimum heavy-atom distance of 4 Angstrom or less; bars are the replicate mean and error bars the standard deviation across three replicas, and Lys155 shows zero occupancy in all three systems. (F) Per-residue C-alpha RMSF, replicate mean and standard deviation across three replicas, for the overall mean and for Phe185 and Tyr217.

Supplementary Files

This is a list of supplementary files associated with this preprint. Click to download.

- S1File.docx